HHS Public Access

Author manuscript

J Am Chem Soc. Author manuscript; available in PMC 2021 January 29.

Published in final edited form as:

J Am Chem Soc. 2020 January 29; 142(4): 1680–1685. doi:10.1021/jacs.9b10993.

Rosette Nanotube Porins as Ion Selective Transporters and Single-Molecule Sensors

Prabhat Tripathi[1], **Liang Shuai**[2], **Himanshu Joshi**[6], **Hirohito Yamazaki**[1], **William H. Fowle**[5], **Aleksei Aksimentiev**[6,7], **Hicham Fenniri**[2,3,4], **Meni Wanunu**[1,3,4]

[1]Department of Physics, Northeastern University, Boston, MA, 02115, United States

[2]Department of Chemical Engineering, Northeastern University, Boston, MA, 02115, United States

[3]Department of Chemistry & Chemical biology, Northeastern University, Boston, MA, 02115, United States

[4]Department of Bioengineering, Northeastern University, Boston, MA, 02115, United States

[5]Electron Microscopy Facility, Northeastern University, Boston, MA, 02115, United States

[6]Department of Physics, University of Illinois at Urbana–Champaign, Urbana, Illinois 61801, United States

[7]Beckman Institute for Advanced Science and Technology, University of Illinois at Urbana –Champaign, Urbana, Illinois 61801, United States

Abstract

Rosette nanotubes (RNTs) are a class of materials formed by molecular self-assembly of a fused guanine-cytosine base (G^C base). An important feature of these self-assembled nanotubes is their precise atomic structure, intriguing for rational design and optimization as synthetic transmembrane porins. Here, we present experimental observations of ion transport across 1.1 nm inner diameter RNT porins (RNTPs) of various lengths in the range of 5 – 200 nm. In a typical experiment, custom lipophilic RNTPs were first inserted into lipid vesicles; the vesicles then spontaneously fused with a planar lipid bilayer, which produced stepwise increases of ion current across the bilayer. Our measurements in 1M KCl solution indicate ion transport rates of ~50 ions $s^{-1}V^{-1}$ m, which for short channels amounts to conductance values of ~1 nS, commensurate with naturally occurring toxin channels such as α-hemolysin. Measurements of interaction times of α-cyclodextrin with RNTPs reveals two distinct unbinding timescales, which suggest that interactions of either face of α-cyclodextrin with the RNTP face are differentiable, backed with all-atom molecular dynamics simulations. Our results highlight the potential of RNTPs as self-assembled non-proteinaceous single-molecule sensors and selective nanofilters with tunable functionality through chemistry.

aksiment@illinois.edu; h.fenniri@northeastern.edu; wanunu@neu.edu.

Supporting Information

Figure S1-S13, Table S1, supplementary methods, additional TEM images of RNTs and RNTPs reconstituted in vesicles, additional data and analysis of RNTP conductance, sensing data of α-CD, and MD simulation details.

Graphical Abstract

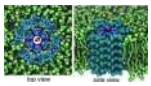

Intrigued by nature's biochemical machinery,[1,2] scientists have been trying to create *de novo* design of trans-membrane channels that can be engineered and tuned to exhibit selective transport of ions and molecules, sense and recognize specific chemicals/biomolecules, and behave as actuatable gates that open and close in response to various stimuli.[3] Indeed, numerous conventional building blocks such as polypeptides[4,5] and organic polymers[6] have been used to produce mimics of biological channels and transporters, although *de novo* design is enormously challenging because polymer folding is often difficult to predict and poor solubility in water can complicate experiments.[7,8] While several examples of self-assembled supramolecular structures were produced,[9,10,11] single-molecule sensing using these pores was not demonstrated, presumably because of their small size (<100 pS conductance values were found in 1–2 M KCl electrolytes). To generate larger self-assembled pores, origami-based folding of DNA into well-defined and predictable transmembrane channels has been achieved recently,[12,13,14] and further utilized for single-molecule sensing.[15] However, issues that remain with DNA-based nanopores include a high cost and low yield of manufacturing the DNA precursors, possibilities of misfolding via incorrect hybridization to the staple DNA oligomers, as well as ion leakage through the skeleton of the DNA pores.[16,17] Recent works suggest that a DNA duplex spanning the lipid bilayer can also produce an ion current,[18] further proof of the leaky nature of DNA to ions.[19] In principle, for *de novo* design of transmembrane channels, molecular building blocks should be as small as possible and should be organized together with strong forces to provide a stable, rigid, and well-defined nanostructure.

The discovery of hierarchical self-assembly of heteroaromatic bicyclic G^C base (Figure 1A) allows us to create predictable and rigid rosette nanotube porins (RNTPs) with tunable dimensions and chemical/physical properties.[20.21] RNTPs can be promising alternatives to top-down pore structures, as the molecules that self-assemble into RNTPs are relatively straightforward. Recently, carbon nanotube porins have been incorporated in lipid bilayer and in live cell membranes to explore water and ion transport.[22,23] Here, we measure the ion transport properties of RNTPs by creating synthetic channels constructed entirely from the self-assembly of bicyclic base G^C, anchored into planar lipid bilayers through porphyrin side chains. The bicyclic system G^C undergoes a hierarchical self-assembly process. First, it forms a six-membered rosette-like ring (Figure 1B), stabilized by 18 H-bonds.[20,21] Several rosettes rings then organize *via* π-π stacking to produce an arbitrary-length RNTP with an internal diameter of 1.1 nm, resulting in barrel-like architecture (Figure 1C).[21] Because of the presence of porphyrin moieties, the RNTPs easily partition into lipid bilayers and are insoluble in water. We overcome this challenge by following recently reported strategies,[12,22] and reconstituting porphyrin modified RNTPs into lipid vesicles, such that fusion of a vesicle into the lipid bilayer results in a transmembrane channel (Figure 1D). We find that RNTPs transport ions at rates of ~50 ions $s^{-1}V^{-1}m$, comparable to previously reported

naturally occurring[1,3] and artificial channels,[4,12,15,22,23] despite the differences in electrostatic and hydrophobic environments of their inner space.

The synthesis of porphyrin-modified heteroaromatic bicyclic base G^C is detailed in the supporting information (S1A). Transmission electron microscopy (TEM) images on RNTP samples established their tubular structure and dimensions (SI: S1E, Figures S2A, S2B). We purified RNTP samples (SI: S1B and Figure S2B) to obtain RNTPs shorter in length and reconstituted them in lipid vesicles (S1C). TEM imaging of RNTPs reconstituted in lipid vesicles show that the RNTPs can stick to lipid bilayer membranes as shown in Figure 2A and Figure S3.

To insert RNTPs in lipid bilayer and explore the transport properties, we formed planar lipid bilayer using Montal-Mueller technique (S1D) on a 50–100 μm aperture on PTFE film separating two compartment cis/trans, each containing 1M KCl, 10mM HEPES, and pH 7.5, and applied an electric potential to the *trans* compartment, keeping *cis* grounded (Figure 1D). Upon addition of 2–5 μL solution of RNTP reconstituted in the vesicle, we observed a stepwise increase in ionic current. We did not observe any ionic current upon addition of vesicles alone. This suggest that the observed stepwise increase in ionic current with RNTP-reconstituted vesicles must be due to the insertion of RNTP in the lipid bilayer. Typical ionic current traces, manifesting the spontaneous insertion of single RNTP in lipid bilayer is shown in Figure 2B and in Figure S4A. Notably, the stepwise jumps in ionic current are not identical in magnitude (Figure S4B), which we attribute to insertions of RNTPs with different lengths. We quantified the length of the inserted RNTPs by measuring the conductance of each inserted channel. The differences in peak positions in the histograms of current traces were taken as single channel currents (Figures 2C, S4A(ii)). The length of inserted RNTPs can be estimated from the conductance of the channels using well-known analytical equations.[24] For example, in Figure 2B, the ionic current jumps from 0.4 ± 0.01 pA to 165 ± 0.04 pA, when an RNTP of conductance 1.64 nS is inserted (L ~ 5.5 nm). The inserted RNTP length distribution (n = 257) is shown in Figure 2C. We performed finite-element COMSOL simulations (Figure S5) to further reinforce the conductance/length relationship in these RNTPs.

Our results have shown that most of the inserted RNTPs are short, less than 20 nm and have a conductance of 1–2 nS (Figure 2D), similar values to biological toxin channels and other reported artificial channels.[4,12,15,22,23] In more than 90% of RNTP insertions, we observed stable and steady-state ionic currents with noise spectra similar to α-hemolysin channels[25] (Figure S6), and lower 1/f noise slopes than for solid-state nanopores[26,27], suggesting that RNTPs are suitable for single-molecule sensing. In less than 10% of cases, we observed unstable and highly stochastic ionic currents (Figure S7), where conductance state of the RNTP fluctuates at different levels. We attribute this behavior to be due to RNTP mis-assembly and/or mechanical instability of a RNTP, akin to gating in biological channels and other synthetic porins such as carbon nanotube porins (CNTPs).[22,23] While in biological channels gating occurs mostly due to conformational changes of proteins, in case of the RNTPs gating can in principle be due to various reasons such as tilting in and out of the lipid bilayer (Figure S7 (ii)). We also observed a class of events where ionic current due to the insertion of several RNTPs decreased in a stepwise manner (Figure S8 (i)), as observed for

DNA barrels in lipid bilayer and interpreted as distinct pore closure events.[14] This effect can also be due to tilting of an RNTP such that the hydrophobic exterior of the RNTPs can be maximally exposed to the lipid environment, as predicted from simulation (See SI: S8).[28]

We also explored the ion selectivity of RNTPs by measuring ionic currents at different transmembrane voltages and salt gradients (Figure 2E). As expected, the current-voltage relationship for RNTPs showed an ohmic behavior at all salt conditions. Selectivity ratios (P_{K^+}/P_{Cl^-}) were calculated at different salt asymmetric conditions from the reversal potentials using the Goldman-Hodgkin-Katz equation (SI: S9). As shown in Table 1, we found a ~2-fold preference for cations over anions at low salt concentrations (<100 mM), and virtually no selectivity at high salt.

To understand the weak cation selectivity, we used molecular dynamics[17] to simulate an all-atom model of an RNTP in a lipid bilayer and surrounded by electrolyte solution. The 150 ns MD trajectory of the system revealed preferential localization of K^+ ions at the center of the nanotube and Cl^- ion in the space between the G^C bases and porphyrin moieties, see Figure 2F, G. Further analysis of the simulation results (SI: S10) reveals on average 750 water molecules and 6 cations (either Na^+ or K^+) within the 5nm long RNTP at steady state.

Finally, we investigated the potential of the RNTPs as robust single-molecule sensors. Here, we employed α-cyclodextrins[29] (α-CD, 200 μM) across the lipid bilayer containing RNTP and observed transient blockades in ionic current. We find that the frequency of ionic current blockades increases with increasing α-CD concentrations (Figures 3A, B). A double exponential fit of the inter-event times distribution (Figure S11(i)) indicates two distinct time constants. This suggests that the individual current blockade events are either due to arrival of single α-CD molecule from bulk to the RNTP or binding/rebinding of the same α-CD to the RNTP. We also observed current blockades at negative voltages (Figure 3D), suggesting that α-CD:RNTP interactions are not voltage polarity dependent. The ionic current blockade lifetimes τ_{off} (Figure 3C) represents the α-CD residence time on the RNTP. The histogram of τ_{off} has a bimodal distribution with two-time constants, ~1 ms and ~5 ms, respectively, and are independent of the applied voltage (Figure 3E, F). This is unlike a charged molecule, where residence times at the pore typically changes with voltage.[30] To understand the observed two types of residence time, we performed all-atom MD simulations of interaction between α-CD and RNTP. The molecular architecture of α-CD is a tapered cylindrical structure with outer diameters 1.46 and 1.37 nm, respectively (Figure 3G, SI: S13). This suggests that α-CD cannot translocate through the RNTP, but can interact with three specific orientations as shown in Figure 3G.

We computed the free-energy between an α-CD molecule and an RNTP for the approach of an α-CD molecule to an RNTP in three different orientations (Figure 4). Looking at the depth of the free energy well near the RNT entrance, we find that conformation 3 (see Figure 3G), in which the primary carbon of the glucose moieties interacts with the RNT face, has a higher affinity than the other two conformations. Consequently, we attribute the time constant τ_{off2} in Figure 3E to a binding mode representing conformation 3, and τ_{off1} to conformations 1 and/or 2.

Our results establish RNTPs as promising *de novo* porins with predefined diameters. More work is needed to demonstrate controllable chemical and physical properties, as well as to improve porin lifetimes from several minutes to hours of operation. In addition, we have demonstrated here single-molecule sensing of α-CD, a chiral molecule, revealing differential interaction times for both faces of the molecule with the achiral RNTP face. We expect that RNTP improvements could lead to new porins with enhanced ion selectivity, which can pave the way to new directions for water purification applications, industrial-scale separations, or flexible reconfigurable nanofluidic circuits. For example, the inner channel of RNTP can be functionalize with a variety of hydrophobic, aromatic, or hydrophilic groups to further tune the selectivity (work in progress). Moreover, inserting one or two rings between the G and C faces of the G^C base[31–32] should also allow for the design of transmembrane channel structures with larger pore diameters (1.4 nm and 1.7 nm) that can perhaps achieve single-file translocation and sequence-selective sensing of biopolymers such as nucleic acids and proteins.[33]

Supplementary Material

Refer to Web version on PubMed Central for supplementary material.

ACKNOWLEDGMENTS

We would like to thank Xinqi Kang for her assistance with experiments with the lipid vesicles. We would like to thank Dr. Naresh Niranjan Dhanasekar for helpful discussion on TEM imaging of vesicles. This work was supported by the National Science Foundation (DMR-1710211, MW). HJ and AA acknowledge support from the National Institutes of Health (P41-GM104601), National Science Foundation (DMR-1827346), and supercomputer time provided through XSEDE Allocation Grant MCA05S028 and the Blue Waters petascale supercomputer system (UIUC).

REFERENCES AND NOTES

1. Hille B, Ion Channels of Excitable Membranes. 2001, Sinauer, Sunderland, MA, ed. 3.
2. Sui H; Han BG; Lee JK; Walian P; Jap BK, Structural basis of water-specific transport through the AQP1 water channel. Nature 2001, 414, 872–878. [PubMed: 11780053]
3. Bayley H; Cremer PS, Stochastic sensors inspired by biology. Nature 2001, 413, 226–230. [PubMed: 11557992]
4. Ghadiri MR; Granja JR; Buehler LK, Artificial transmembrane ion channels from self-assembling peptide nanotubes. Nature 1994, 369, 301–304. [PubMed: 7514275]
5. Montenegro J; Ghadiri MR; Granja JR, Ion channel models based on self-assembling cyclic peptide nanotubes. Accounts of Chemical Research 2013, 46, 2955–2965. [PubMed: 23898935]
6. Sakai N; Matile S, Synthetic Ion Channels. Langmuir 2013, 29, 9031–9040. [PubMed: 23631769]
7. Litvinchuk S; Tanaka H; Miyatake T; Pasini D; Tanaka T; Bollot G; Mareda J; Matile S, Synthetic pores with reactive signal amplifiers as artificial tongues. Nat. Mater, 2007, 06, 576–580.
8. Thomson AR; Wood CW; Burton AJ; Bartlett GJ; Sessions RB; Brady RL; Woolfson DN, Computational design of water-soluble α-helical barrels. Science 2014, 346, 485–488. [PubMed: 25342807]
9. Sakai N; Kamikawa Y; Nishii M; Matsuoka T; Takashi K; Matile S, Dendritic folate rosettes as ion channels in lipid bilayers. J. Am. Chem. Soc. 2006, 128, 2218–2219. [PubMed: 16478168]
10. Saha T; Dasari S; Tewari D; Prathap A; Sureshan KM; Bera AK; Mukherjee A; Talukdar P, Hopping-mediated anion transport through a mannitol-based rosette ion channel. J. Am. Chem. Soc., 2014, 136, 14128–14135. [PubMed: 25203165]

11. Saha T; Gautam A; Mukherjee A; Lahiri M; Talukdar P, Chloride transport through supramolecular barrel-rosette ion channels: Lipophilic control and apoptosis-inducing activity. J. Am. Chem. Soc. 2016, 138, 16443–16451. [PubMed: 27933857]
12. Langecker M; Arnaut V; Martin TG; List J; Renner S; Mayer M; Dietz H; Simmel FC, Synthetic lipid membrane channels formed by designed DNA nanostructures. Science 2012, 338, 932–936. [PubMed: 23161995]
13. Burns JR; Stulz E; Howorka S, Self-assembled DNA nanopores that span lipid bilayers. Nano Lett. 2013, 13, 2351–2356. [PubMed: 23611515]
14. Burns JR; Gopfrich K; Wood JW; Thacker VV; Stulz E; Keyser UF; Howorka S, Lipid-bilayer-spanning DNA nanopores with a bifunctional porphyrin anchor. Angew. Chem. Int. Ed. 2013, 52, 12069 –12072.
15. Burns JR; Seifert A; Fertig N; Howorka S, A biomimetic DNA-based channel for the ligand-controlled transport of charged molecular cargo across a biological membrane. Nat. Nanotechnol. 2016, 11, 152–156. [PubMed: 26751170]
16. Pinheiro AV; Han D; Shih WM; Yan H, Challenges and opportunities for structural DNA nanotechnology. Nat. Nanotechnol. 2011, 06, 763–772.
17. Yoo J; Aksimentiev A, Molecular dynamics of membrane-spanning DNA channels: Conductance mechanism, electro-osmotic transport, and mechanical gating. J. Phys. Chem. Lett. 2015, 6, 4680–4687. [PubMed: 26551518]
18. Gopfrich K; Li CY; Mames I; Bhamidimarri SP; Ricci M; Yoo J; Mames A; Ohmann A; Winterhalter M; Stulz E; Aksimentiev A; Keyser UF, Ion channels made from a single membrane-spanning DNA duplex. Nano Lett. 2016, 16, 4665–4669. [PubMed: 27324157]
19. Krishnan S; Ziegler D; Arnaut V; Martin TG; Kapsner K; Henneberg K; Bausch AR; Dietz H; Simmel FC, Molecular transport through large-diameter DNA nanopores. Nat. Commun. 2016, 7, 12787. [PubMed: 27658960]
20. (a)Fenniri H; Mathivanan P; Vidale KL; Sherman DM; Hallenga K; Wood KV; Stowell JG, Helical Rosette Nanotubes: Design, Self-Assembly, and Characterization. J. Am. Chem. Soc. 2001, 123, 3854–3855, [PubMed: 11457132] (b)Fenniri H; Deng BL; Ribbe AE; Hallenga K; Jacob J; Thiyagarajan P, Entropically driven self-assembly of multichannel rosette nanotubes. Proc. Natl. Acad. Sci. USA, 2002, 99, 6487–6492. [PubMed: 11891281]
21. (a)Beingessner R; Deng B-L; Fanwick PE; Fenniri H, A Regioselective Approach to Trisubstituted 2 (or 6)-Arylaminopyrimidine-5-carbaldehydes and Their Application in the Synthesis of Structurally and Electronically Unique G^C Base Precursors. J. Org. Chem. 2008, 73, 931–939. [PubMed: 18179232] (b)Fenniri H; Tikhomirov GA; Brouwer DH; Bouatra S; El-Bakkari M; Yan Z; Cho J-Y; Yamazaki T, High Field Solid-State NMR Spectroscopy Investigation of 15N-Labeled Rosette Nanotubes: Hydrogen Bond Network and Channel-Bound Water. J. Am. Chem. Soc. 2016, 138, 6115–6118. [PubMed: 27141817] (c)Hemraz UD; El Bakkari M; Yamazaki T; Cho J-Y; Beingessner RL; Fenniri H, Chiromers: Conformation-driven mirror-image supramolecular chirality isomerism identified in a new class of helical rosette nanotubes. Nanoscale 2014, 6, 9421–9427. [PubMed: 24770905]
22. Geng J; Kim K; Zhang J; Escalada A; Tunuguntla R; Comolli LR; Allen FI; Shnyrova AV; Cho KR; Munoz D; Wang YM; Grigoropoulos CP; Ajo-Franklin CM; Frolov VA; Noy A, Stochastic transport through carbon nanotubes in lipid bilayers and live cell membranes. Nature 2014, 514, 612–615. [PubMed: 25355362]
23. Tunuguntla R; Henley RY; Yao YC; Pham TA; Wanunu M; Noy A, Enhanced water permeability and tunable ion selectivity in subnanometer carbon nanotube porins. Science 2017, 357, 792–796. [PubMed: 28839070]
24. $G = \sigma\left[\frac{4l}{\pi d^2} + \frac{1}{d}\right]$, G = conductance of the pore, σ is bulk conductivity of electrolyte solution, l is length of the pore, and d is the diameter of the pore. For 1M KCl σ is 110mS/cm, and for RNTP, d is 1.1 nm. Therefore, RNTP length can be derived as $l = 0.8635\left[\frac{12.1}{G} - 1\right]$, where G is in nS and l is in nm.

25. Kasianowicz JJ; Bezrukov SM; Protonation dynamics of the α-toxin ion channel from spectral analysis of pH-dependent current fluctuations. Biophysical Journal, 1995, 69, 94–105. [PubMed: 7545444]

26. Fragasso A; Pud S; Dekker C; 1/f noise in solid-state nanopores is governed by access and surface regions. Nanotechnology. 2019, 30, 395202.

27. Parkin WM; Drndic M; Signal and noise in FET-nanopore Devices. ACS Sens. 2018, 3, 313–319. [PubMed: 29322780]

28. Lopez CF; Nielsen SO; Moore PB; Klein ML, Understanding nature's design for a nanosyringe. Proc. Natl. Acad. Sci. USA. 2004, 101, 4431–4434. [PubMed: 15070735]

29. Gu LQ; Braha O; Conlan S; Cheley S; Bayley H; Stochastic sensing of organic analyte by a pore-forming protein containing a molecular adapter. Nature, 1999, 398, 686–690. [PubMed: 10227291]

30. Kasianowicz JJ; Brandin E; Branton D; Deamer DW, Characterization of individual polynucleotide molecules using a membrane channel. Proc. Natl. Acad. Sci. USA, 1996, 93, 13770–13773. [PubMed: 8943010]

31. Borzsonyi G; Beingessner RL; Yamazaki T; Cho J; Myles AJ; Malac M; Egerton R; Kawasaki M; Ishizuka K; Kovalenko A; and Fenniri H, Water-soluble J-type rosette nanotubes with giant molar ellipticity. J. Am. Chem. Soc. 2010, 132, 15136–15139. [PubMed: 20936820]

32. Borzsonyi G; Alsbaiee A; Beingessner RL; Fenniri H, Synthesis of a tetracyclic G^C scaffold for the assembly of rosette nanotubes with 1.7 nm inner diameter. J. Org. Chem. 2010, 75, 7233–7239. [PubMed: 20929202]

33. Piguet F; Ouldali H; Pastoriza-Gallego M; Manivet P; Pelta J; Oukhaled A; Identification of single amino acid differences in uniformly charged homopolymeric peptides with aerolysin nanopore. Nat Commun. 2018, 9, 966. [PubMed: 29511176]

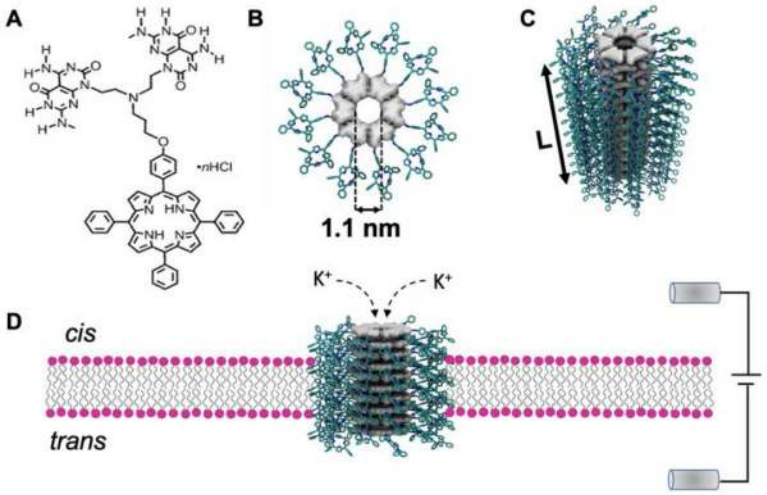

Figure 1. Synthetic rosette nanotube porins (RNTPs) in lipid bilayer *de novo* from fused G^C base.

(A) Chemical structure of fused porphyrin modified G^C base. (B) Top view of rosette stack formed *via* hydrogen bonding of six G^C bases. (C) Perspective view of a RNTP of length L, formed by π-π stacking of several rosettes. (D) RNTP insertion into the lipid bilayer results in a water-filled RNTP lumen. Application of voltage across the membrane results in ion flow across the pore, as shown here for K^+ ions.

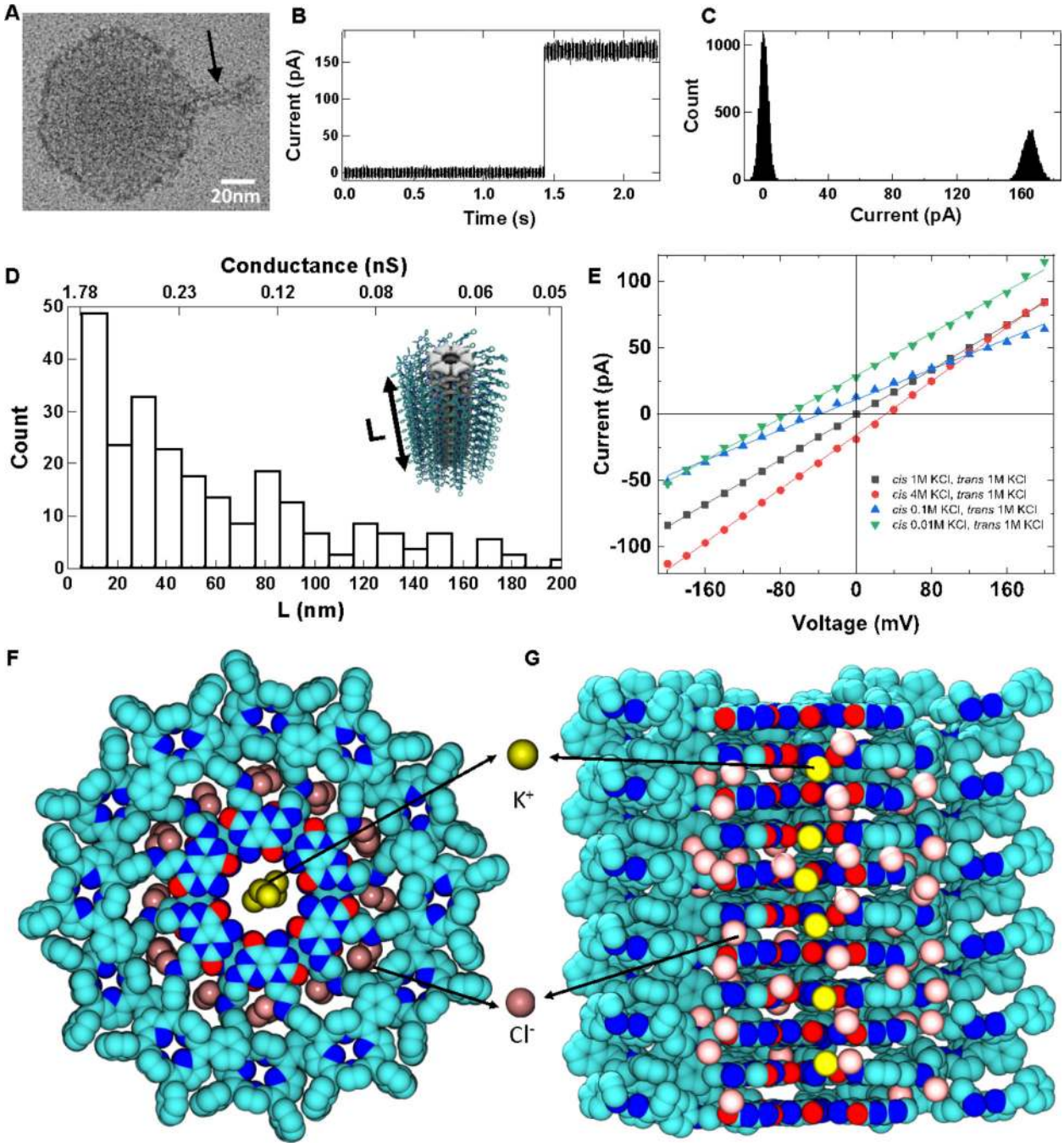

Figure 2. Ion conductance of RNTPs.

(A) Representative TEM image of a ~40 nm long RNTP reconstituted in a lipid vesicle (see black arrow). (B) Observation of a step-wise increase in ion current due to incorporation of single RNTP in lipid-bilayer of estimated length 5.5 nm. The traces shown here were recorded at 1 M KCl, 10 mM HEPES, pH 7.5 at 100 mV and current signal was low-pass filtered at 5 kHz (C) All-point histogram of the current trace shown in (B). (D) Histogram of estimated RNTP lengths (L) based on data from 257 insertions. (E) Current vs voltage for different salt conditions for a ~25-nm long RNTP. A snapshot from the all-atom MD

simulation of an ~ 5nm long RNTP showing the (F) top and (G) side views. The non-hydrogen atoms of RNTP are shown as spheres colored according to atom type (carbon in cyan, nitrogen in blue, oxygen in red); Cl^- and K^+ are shown as pink and yellow spheres, respectively. Water and lipid molecules are not shown for clarity. The snapshot shows that the cations are only present in the central channel lumen, and the anions are distributed in the periphery of the channel. The simulation explains the weak selectivity of RNTP towards K^+ transport due to binding of Cl^- to positively charged ammonium groups at the junction of G^C bases and porphyrin.

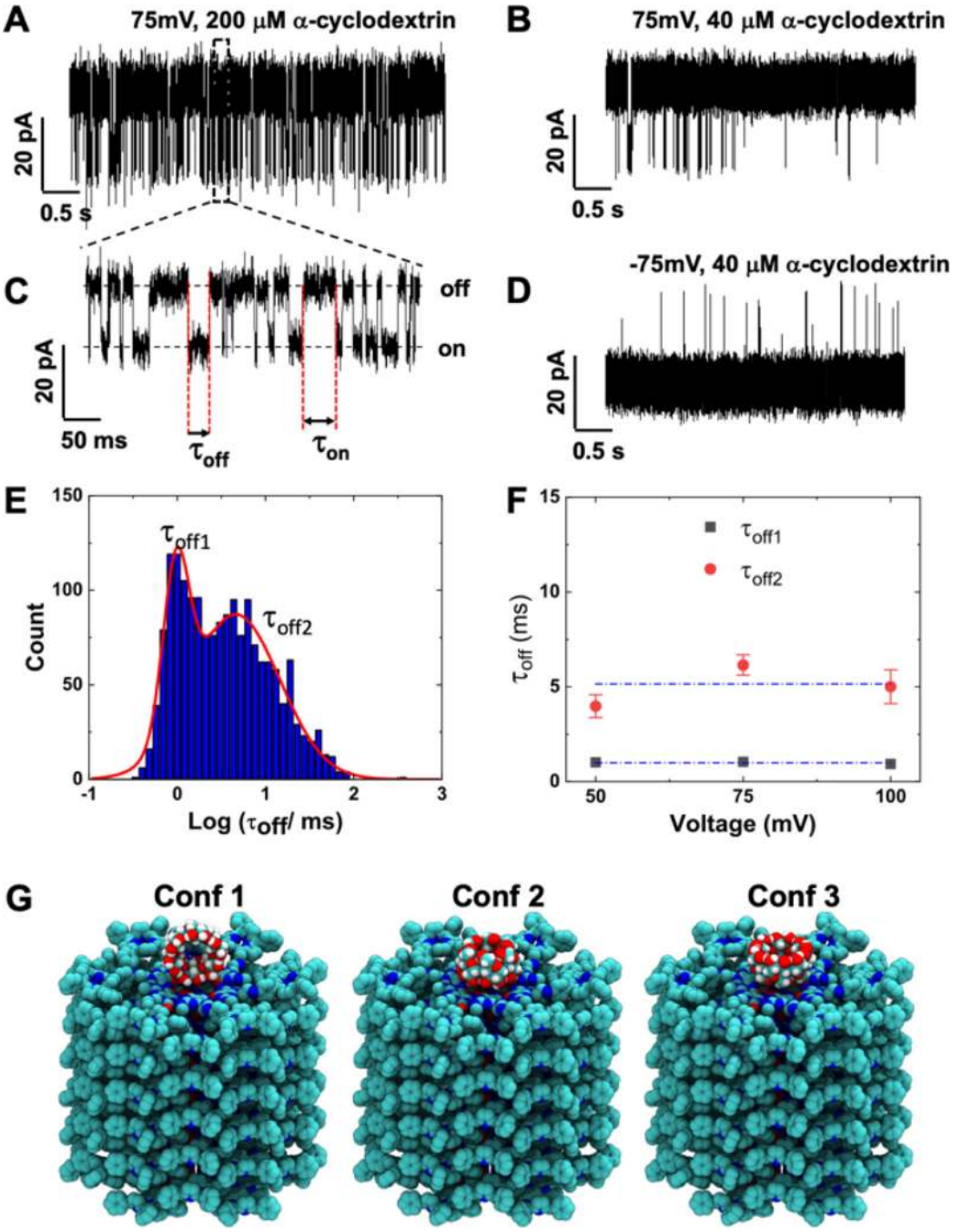

Figure 3. Single-molecule sensing of α-cyclodextrin (α-CD) with RNTP.

(A) Trace of ionic current blockades induced by 200 μM α-CD at 75 mV. (B) Trace of ionic current blockades induced 40 μM α-CD at 75 mV. (C) Zoomed-in view of the trace in A, showing distinct current blockades induced by the interaction of α-CD with an RNTP. The lifetime τ_{off} is the duration of time α-CD stays at the RNTP ("on" state) before unbinding. The lifetime τ_{on} represents the time that α-CD takes to arrive and bind to the RNTP. (D) Trace showing ionic current blockades for 40 μM α-CD at −75 mV. Current traces shown in plots were recorded at 1M KCl, 10mM HEPES, pH 7.5, and low-pass filtered at 5kHz. (E)

Histogram of τ_{off} times, n=1,752. Red curves represent the fit of histogram with a double-peak gaussian function. F) Peak positions of the histogram (τ_{off1} and τ_{off2}) as a function of applied voltage. Error bars represents standard error obtained in fitting with two peak gaussian function. (G) Snapshots of all atom MD simulation of the three conformations (1, 2, and 3) of α-CD at the RNTP. The simulation results show that conformation 3 has strongest interaction with the RNTP. Blockade currents computed using the Steric Exclusion Model (SI: S15) for the various conformations are 18, 51 and 51 % of the open pore value, consistent with our experimental data.

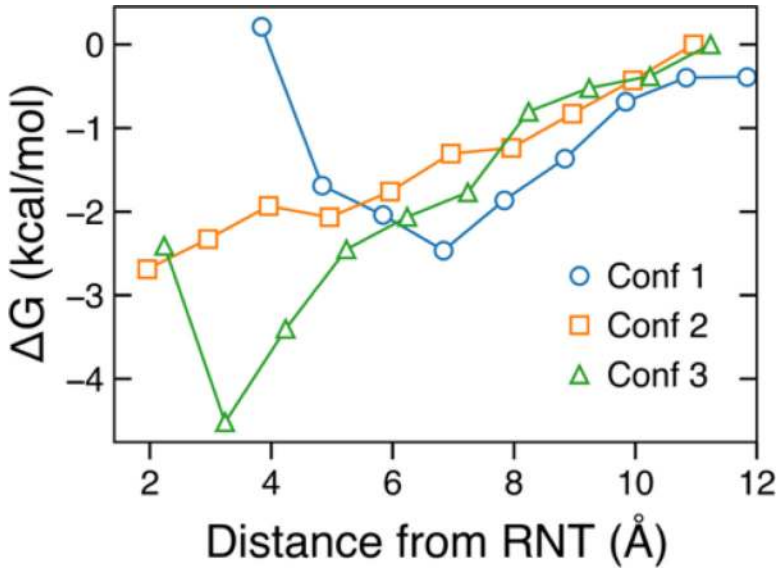

Figure 4. Energetics of α-CD and RNTP interactions.

Free energy as a function of distance between the center-of-mass of α-CD and the top layer of an RNTP for three specific conformations shown in 3G (see text).

Table 1.

Reversal potentials and selectivity ratios of RNTPs measured under different KCl concentration gradients (pH 7.5).

Salt concentration (cis/trans)	Corrected V_R (mV)	Permselectivity	Selectivity ratio (K^+/Cl^-)
0.01M/1M	37.9	0.35	2.03
0.1M/1M	15.5	0.31	1.82
4M/1M	−2.7	0.09	1.17